Ionic conductances in sustentacular cells of the mouse olfactory epithelium

Fivos Vogalis, Colleen C. Hegg and Mary T. Lucero

Department of Physiology, University of Utah, 410 Chipeta Way, Salt Lake City, UT 84108-1297, USA

The electrical properties of sustentacular cells (SCs) in the olfactory epithelium (OE) were investigated in tissue slices taken from neonatal mice (P0–P4). Conventional whole-cell recordings were obtained from SCs and also from olfactory receptor neurones (ORNs) *in situ*. SCs had a larger apparent cell capacitance (C_{cell}) (18.6 ± 0.5 pF) than ORNs (4.4 ± 0.4 pF) and a lower apparent membrane resistance (R_m) (160 ± 11 MΩ *versus* 664 ± 195 MΩ, respectively). When corrected for a seal resistance of 1 GΩ, these mean R_m values were increased to 190 MΩ and 2 GΩ in SCs and ORNs, respectively. SCs generated a TTX (1 μM)-resistant voltage-activated Na^+ current (I_{Na}) that had a peak density at −38 mV of −44 pA pF^{-1} and supported action potential firing. Peak current density of I_{Na} in neurones was 510 ± 96 pA pF^{-1}. The outward K^+ current in SCs was composed (> 70%) of a TEA (2 mM)-sensitive component that was mediated by the opening of large-conductance (237 ± 10 pS; BK) channels. The resting leak conductance (g_L) of SCs was permeable to monovalent cations and anions and was largely inhibited by substitution of external Na^+ with NMDG and by internal F^- with gluconate. g_L deactivated up to 50% at potentials negative of −70 mV and was inhibited by 18β-glycyrrhetinic acid (20 μM). SCs were identified using fluorescent dyes (Lucifer Yellow and Alexa Fluor 488) in the whole-cell patch pipette-filling solution. Our findings indicate that SCs in the OE of neonates are electrically excitable and are distinguishable from neurones by a having a resting g_L.

(Resubmitted 12 November 2004; accepted after revision 3 December 2004; first published online 20 December 2004)
Corresponding author M. T. Lucero: 410 Chipeta Way, Room 156, University of Utah, Salt Lake City, UT 84108-1297, USA. Email: mary.lucero@m.cc.utah.edu

The olfactory epithelium (OE) is functionally defined by the odourant-sensing properties of olfactory receptor neurones (ORNs). Sustentacular cells (SCs) comprise another major population of OE-resident cells but have been less well studied in vertebrates. SCs form a tightly packed columnar monolayer on the apical surface of the OE and are known to be involved in the secretion of mucus, biotransformation of noxious chemicals, phagocytosis of dead ORNs and in buffering of extracellular K^+ (Getchell & Getchell, 1982; Getchell & Mellert, 1991). Functionally, SCs share common features with glial cells and epithelial cells and may serve similar roles in the OE.

In keeping with their glial-like function, SCs are thought to possess K^+ channels and ion transporters to enable them to buffer extracellular K^+. In the OE of the frog, for example, SCs possess large-conductance Ca^{2+}-activated K^+ (BK) channels (Trotier, 1998) which are activated by increases in intracellular [Ca^{2+}] and by membrane depolarization. A more recent study on SCs dissociated from the murine vomeronasal organ (VNO), a region structurally similar to the OE, showed that SCs possessed voltage-gated outward K^+ channel currents and also a conspicuous voltage-gated inward Na^+ current (Ghiaroni *et al.* 2003). Voltage-gated Na^+ currents are also found in glial cells although their exact function is not clear since glial cells, like SCs in the VNO, are not capable of generating action potentials (Verkhratsky & Steinhauser, 2000). Another difference that has been reported between neurones and sustentacular cells dissociated from the VNO is that SCs have a disproportionately lower input resistance than neurones (Ghiaroni *et al.* 2003). Whether this is also a feature of SCs in the olfactory epithelium has not been investigated.

In the present study we examined the electrical properties of SCs situated within OE slices taken from neonatal mice (P0–P4). We characterized the major voltage-gated ionic currents in SCs *in situ* when filled with fluorescent dye under whole-cell recording conditions. Our results indicate that SCs in OE slices from neonatal mice are capable of regenerative activity when a resting 'leak' conductance is inhibited. The ionic nature of this resting conductance and the implications on SC function are discussed. The results of this study have been presented in abstract form (Vogalis *et al.* 2005).

 DOI: 10.1113/jphysiol.2004.079228

Methods

Preparation of OE slices for patch clamp recording

Coronal slices of olfactory epithelium, 250 μm in thickness, were prepared from neonatal Swiss Webster mice (P0–P4), as previously described (Hegg & Lucero, 2001; Hegg *et al.* 2003). Briefly, mouse pups were killed by decapitation using a sharp blade and the skin covering the head was removed by dissection. All animal procedures were approved by the University of Utah Institutional Animal Care and Use Committee. Slices were pinned out on to a 12-mm coverslip coated with elastomer (Sylgard, Dow Corning, USA) and placed in a tissue perfusion chamber (ca 0.25 ml in volume), on an upright fluorescence microscope (Nikon). The slice was perfused ($\sim$1 ml min^{-1}) with Ringer solution at room temperature (21–23°C) for 1 h before recording.

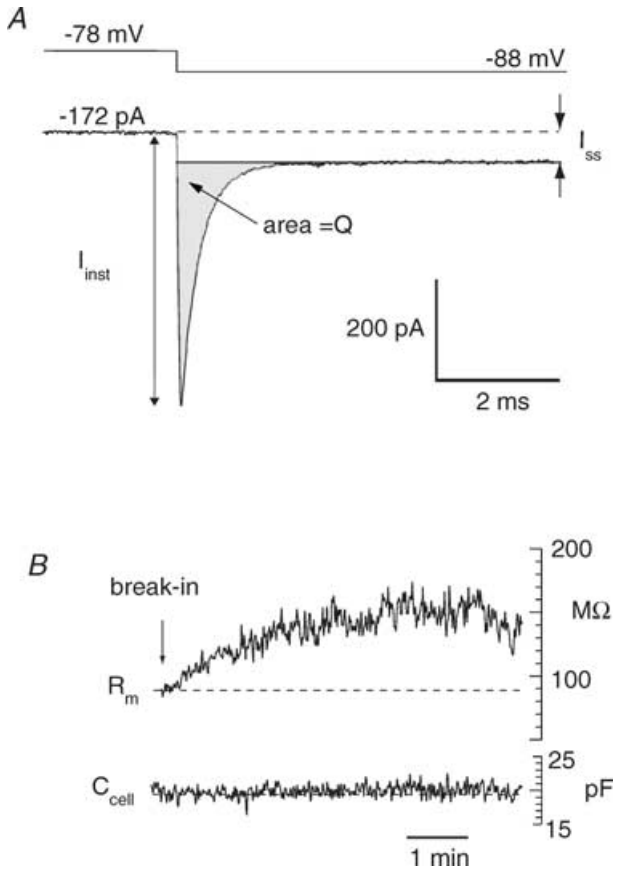

Figure 1. Measurement of apparent membrane resistance (R_m) and apparent cell capacitance (C_{cell}) of sustentacular cells (SCs) in slices of olfactory epithelium (OE)

A, whole-cell recording of the capacitive current (I_C) (lower trace) elicited by 10 mV hyperpolarizing steps (V_{step}) from a holding potential of −78 mV (upper trace). The parameters of I_C that were measured were the peak current excursion (I_{inst}), the steady-state current (I_{SS}) and the time integral of I_C which represents the charge displaced (Q). The following equations were used to measure R_m and C_{cell}:

$$R_m = (V_{step} - (V_{step}/I_{inst})I_{ss})/I_{ss}$$
$$C_{cell} = Q/(V_{step} - (V_{step}/I_{inst})I_{ss}).$$

B, increase in R_m following whole-cell access (upper trace) while C_{cell} is unchanged. R_m and C_{cell} were calculated from recordings of I_C elicited by 10 ms V_{step} pulses delivered at 2 Hz.

Patch pipettes were made from borosilicate thick-walled glass tubing (ID 0.87 mm, OD 1.15 mm; Sutter) and pulled to have resistances of 5–8 MΩ when filled with internal pipette-filling solutions. The bath was grounded with a 3 M KCl–agar bridge and a Ag–AgCl wire. To minimize pipette capacitance artifacts, the depth of the bath was kept to a minimum. Currents were recorded and voltage command potentials were applied to cells using an Axopatch 200A amplifier (Axon Instruments), driven by Clampex 8.2 (Axon Instruments), running on a dedicated PC. Capacitive currents were subtracted on-line by applying a P/4 subtraction protocol. Voltage-gated currents were low-pass filtered at 10 kHz and sampled at 20 kHz, while 'leak' currents were sampled at 1 kHz. Patch recordings were low-pass filtered at 1 kHz and sampled at 5 kHz. Further analysis of the data was performed using Clampfit 8.2 (Axon Instruments) and Igor 4.0 software (Wavemetrics, OR, USA) and measurements were stored as Excel spreadsheets.

Cells that were filled with the fluorescent dyes dissolved in the pipette-filling solution (Lucifer Yellow, 0.2%; Alexa Fluor 488, hydrazine salt, 100 μM) were visualized using a B2A filter block (450–490 nm excitation and 520 nm barrier filters). Fluorescence images of cells and bright field images of the slices were captured using a digital camera (DP10, Olympus) attached to the microscope. Images were digitally enhanced and merged using Photoshop 6.0 and Illustrator 9 (Adobe). Where noted, some slices were transferred to the stage of a confocal laser microscope (Zeiss LSM510; excitation beam: 488 nm; emission long-pass filter: 510 nm) and images were captured using the LSM 510 software.

SCs were patched by positioning the tip of the pipette adjacent to the apical surface of the OE using a micromanipulator (MP-225, Sutter) and then slowly advancing the electrode towards the surface. For consistency, recordings were obtained from the region corresponding to the dorsal nasal cavity. Positive pressure was applied until contact with the outermost cell layer and a high-resistance seal (0.5–2 GΩ) was allowed to form before the membrane was ruptured to establish the whole-cell recording configuration. All recordings were performed at room temperature (21–23°C).

Measurement of the apparent cell capacitance (C_{cell}), apparent membrane resistance (R_m) and series resistance (R_s) was performed off-line, from recordings of capacitive current (I_C) elicited by 10 ms, 10 mV step hyperpolarizations from a holding potential of −78 mV, using an Igor Procedure file (Fig. 1*A*). Pipette capacitive currents were nulled prior to seal formation. Recordings from SCs could be distinguished from ORNs because SCs had larger values of C_{cell} ($>$ 10 pF) and lower values of R_m. In

addition, ORNs generated much larger inward currents in the nanoamp range. Following whole-cell access, the R_m of SCs increased from an initially low level (< 50 MΩ) up to 100–150 MΩ over the ensuing 5–10 min (Fig. 1*B*). Therefore recordings were commenced after a 5–10 min equilibration period. Series resistance compensation was not used. The majority of cells that were filled with fluorescent dye generally conformed to the morphology of SCs (see Fig. 2*A* and *C*).

Perfusion solutions and internal pipette-filling solutions

The standard Ringer solution used to perfuse slices consisted of (mM): NaCl, 140; KCl, 5; $MgCl_2$, 1; $CaCl_2$, 2; Hepes, 10; glucose, 10; pH 7.4, 330 mosmol l^{-1}. NMDG-Ringer solution contained 140 mM *N*-methyl-D-glucamine in place of NaCl, and was adjusted to pH 7.4 with HCl. We used a number of different internal pipette-filling solutions. The standard internal solution (KF) had the following composition (mM): KF, 125; KCl, 15; $MgCl_2$, 3; Hepes, 10; EGTA, 11; pH 7.2 with KOH. A sodium gluconate internal solution consisted of 145 mM sodium gluconate in place of KCl and KF, and also contained (mM): $MgCl_2$, 1; Hepes, 10; EGTA, 11; pH was adjusted to 7.2 with NaOH. To minimize current flow through K^+ channels and record Na^+ channel currents, a CsF-based internal solution was also used which consisted of (mM): CsF, 125; CsCl, 15; $MgCl_2$, 1; $CaCl_2$, 1; EGTA, 2.5; Hepes, 10; ATP-K_4, 2; GTP-Li, 0.2; pH 7.2 with CsOH. Where noted, in some recordings, we also used a KCl-based internal solution containing 140 mM KCl, and 0.5 mM EGTA with no added Ca^{2+}. The KF-based internal solution provided the most stable recordings.

Liquid junction potentials (LJPs) were calculated using JPCalc in Clampex (Barry & Diamond, 1970) and equalled 8 mV for KF internal solution and 9 mV for CsF internal solution. These values have been subtracted from measurements of voltage, unless otherwise stated. In addition, the LJP following wash-in of NMDG-Ringer external solution was equal to 9 mV in CsF-loaded cells while the LJP between the sodium gluconate internal solution and Ringer solution was 13 mV. These values were taken into account when interpreting the permeability of ionic conductances calculated from shifts in the E_{rev} of the relevant currents (see Results). Relative permeabilities of ions were determined from the E_{rev} under bi-ionic conditions, or from changes in E_{rev} upon substitution of one ion for another in the external solution (Hille, 1992).

Drugs and other chemicals

All the reagents used for making bathing solutions and internal pipette solutions were purchased from Sigma unless indicated otherwise. 1-Octanol was diluted in Ringer solution and vortexed before perfusion. Niflumic acid was dissolved in DMSO as a 1 M stock, as was 9-anthracene carboxylic acid (9-AC) and then diluted in Ringer solution (final [DMSO], 7 μM; 5.46×10^{-5}%). 18β-glycyrrhetinic acid was dissolved in ethanol as a 0.1 M stock (final [ethanol], 0.15 mM; 0.015%). Neither the DMSO nor ethanol had significant effects on cells at the dilutions used. Tetrodotoxin (TTX, 1 μM) was dissolved directly in Ringer solution. Tetraethylammonium chloride (TEA) was made up as a 1 M stock solution which was added to the perfusate. Charybdotoxin (CHTX) was a gift from NPS Pharmaceuticals (Salt Lake City, UT, USA) and was stored frozen (−80°C) in 25 μl aliquots which were added to the tissue chamber.

Statistical tests and data handling

The mean values of measurements reported here represent averages computed from '*n*' number of cells. Where measurements were performed on the same cells, before and after a particular treatment, we used the paired Student's *t* test. Otherwise we used Student's *t* test for unpaired observations. In both cases, statistical significance was set at $P < 0.05$, or else the *P* value is given. Curve fitting of the capacitive currents (I_C) and construction of *I–V* relationships and *G–V* relationships was performed using Igor 4.0 (Wavemetrics). For patch recordings (cell-attached and outside-out patches), single channel current amplitude (i) was determined by measuring the current of 10–20 openings and taking the average. All-points histograms were constructed from 30-s segments of recordings using Clampfit (Axon) and fitted with Gaussian curves. From these curves, the open probability of channel opening was determined by summing of the integrated area of each Gaussian curve × the channel level, and dividing this value by the summed area under all the Gaussian curves. Linear regression lines were fitted to data points of i *versus* pipette potential (V_p) to determine unit conductance and reversal potential. Other transformations are noted in the relevant section in the Results.

Results

Morphological features and general electrical properties of apical cells in the OE

Whole-cell recordings were obtained from cells situated on the apical surface of OE slices. A subset of these cells was also filled with fluorescent dye (23 cells filled with 0.2% Lucifer Yellow, LY; 31 cells filled with 100 μM Alexa Fluor 488, AF) which enabled us to image their morphology under UV illumination. Generally there was no apparent difference in the morphology of cells filled with LY or AF (Fig. 2*A* and *C*), although we noted that AF was not as well retained as LY within cells following withdrawal of the

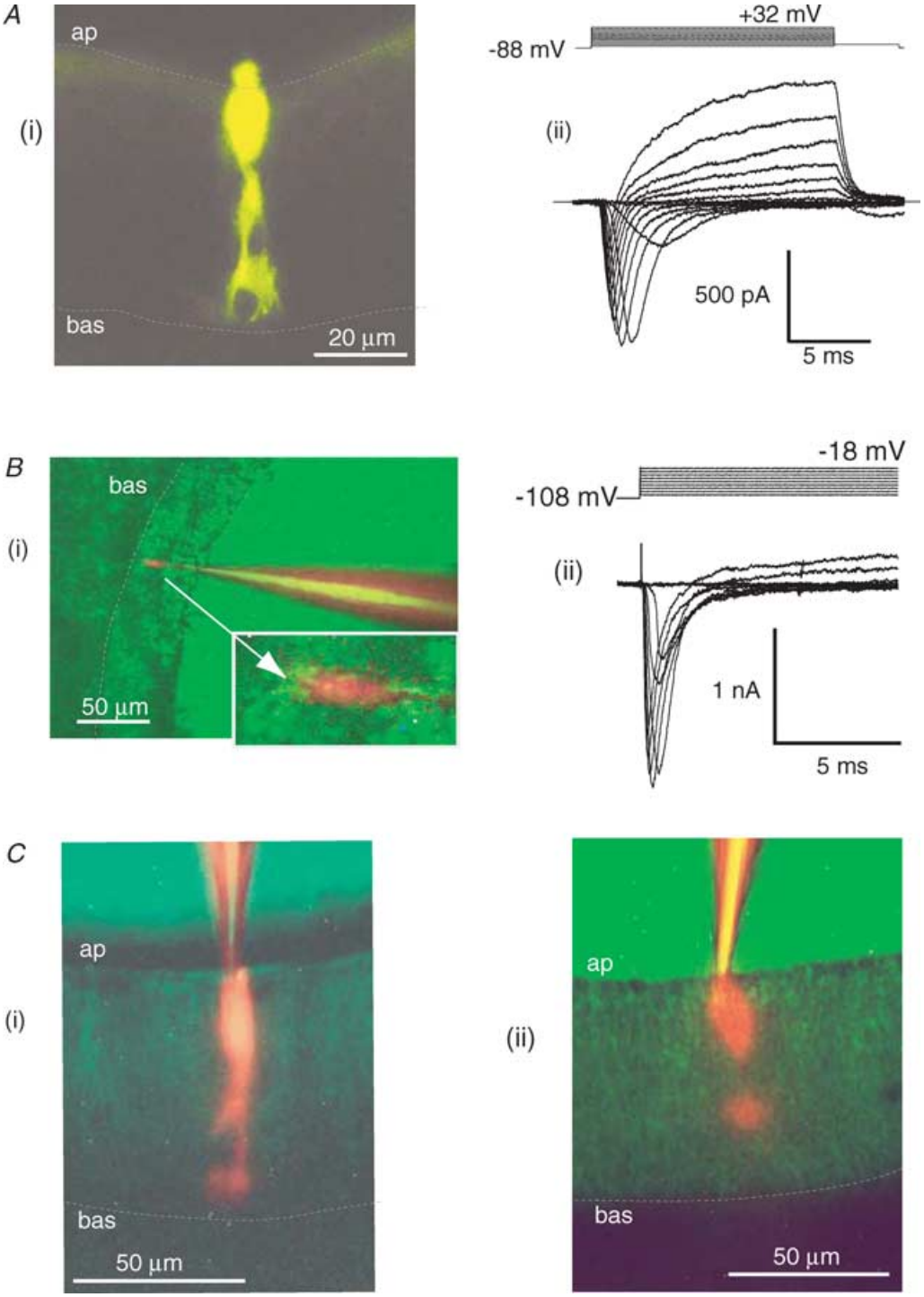

Figure 2. Fluorescent photomicrographs of SCs filled with fluorescent dyes during whole-cell recordings
*A*i, confocal micrograph (10 μm optical slice) of a SC filled with 0.2% Lucifer Yellow showing the cell body lying adjacent to the apical surface (ap) of the OE and the processes projecting across the width of the epithelium towards the basement membrane (bas). ii, whole-cell recordings of inward and outward currents (lower traces) from the same cell. Upper traces represent voltage stimulus protocol; C_{cell}, 14.7 pF; R_m, 210 MΩ. *B*i, fluorescence micrograph of a LY-filled cell in the middle portion of the OE. Inset: enlarged image. ii, whole-cell current recordings from this neuronal-like cell. $C_{cell,}$ 6.7 pF; R_m, 626 MΩ. Note large inward current (lower traces). *C*, fluorescence micrographs of two SCs filled with Alexa Fluor 488 (100 μM) showing the characteristic morphology of SCs.

pipette as the intensity of fluorescence of AF-filled cells diminished within 10 min. Filled cells had oval shaped cell bodies (up to 20 μm in length and 10 μm wide) that were situated along the apical surface. Many of them possessed a thick process or stalk that extended towards the basal region of the OE (Fig. 2*A*i and *C*i) and this process gave rise to thinner 'lamellar' structures that appeared to encircle other cells within the OE. In some filled cells 'end-feet' structures were apparent near the basement membrane. The morphological features revealed by the dyes are consistent with these cells being sustentacular cells (SCs).

Cells situated in the middle third layer of the OE were also patched by advancing the tip of the pipette below the apical surface. One such cell that was filled with LY is shown in Fig. 2*B*i). Despite having a smaller cell body and a smaller cell capacitance, this cell generated an inward current that was two to three times larger than that recorded in SCs (Fig. 2*B*ii). Thus these 'smaller' cells were assumed to be ORNs or immature ORNs. Overall, the average apparent cell capacitance (C_{cell}) of all the SCs that we patch clamped was 18.5 ± 0.5 pF ($n = 156$) while in ORNs C_{cell} averaged 4.4 ± 0.4 pF ($n = 10$). The R_m of SCs averaged 160 ± 11 MΩ ($n = 156$) while in the 10 ORNs R_m averaged at 664 ± 195 MΩ. Both these mean values are likely to underestimate the actual values of R_m in the respective cell types because of the influence of the seal resistance (R_{seal}). Using 1 GΩ as a typical value for R_{seal}, the mean corrected R_m of SCs would be approximately 190 MΩ for SCs and 2 GΩ for ORNs.

In SCs filled with K^+ internal solution, step depolarizations from a holding potential (V_h) of −108 mV to test potentials positive of −60 mV activated time-dependent inward and outward currents (Fig. 3*A*i). The maximum density of inward current was generated at −38 mV and averaged −44 pA pF^{-1} (Fig. 3*A*ii). The maximum density of outward current at +52 mV (measured at the end of 15-ms pulses) was approximately 100 pA pF^{-1} (Fig. 3*A*ii). In contrast, the maximal current density of the inward current recorded in ORNs was about 10-fold greater and averaged 510 ± 96 pA pF^{-1} ($n = 10$) (Fig. 3*A*iii). Despite having a lower density of inward current than ORNs, SCs generated a single action potential (AP) when they were depolarized rapidly to about −60 mV from a holding potential negative of −90 mV (Fig. 3*B*i) and could not be made to fire repetitively by adjusting either the holding current or the strength of the depolarizing current. At their normal resting potential, SCs were not excitable (Fig. 3*B*ii). In contrast, neurones usually generated a burst of action potentials when injected with supra-threshold depolarizing current steps from holding potentials of −90 to −100 mV (Fig. 3*B*iii) (Ma *et al.* 1999). In three SCs examined, the amplitude of APs averaged 71 mV, had a half-amplitude duration of 4.8 ms and a mean overshoot of 15 mV and their resting potentials ranged between −30 and −50 mV.

Voltage-gated Na^+ inward current

Filling SCs with Cs^+ internal solution largely blocked outward K^+ currents and enabled us to record the inward current component in isolation. This was carried exclusively by Na^+ because it was abolished when NMDG was substituted for Na^+ in the Ringer solution (Fig. 4*A*i). In addition, this Na^+ current (I_{Na}) was decreased by TTX (1 μM) by 48% ($n = 3$) (Fig. 4*A*ii), while the same concentration of TTX decreased I_{Na} in ORNs by > 80% ($n = 2$) (Fig. 4*B*). To determine the voltage dependence of I_{Na}, the corresponding conductance (g_{Na}) was plotted as a function of test potential. Conductance was calculated by dividing the mean peak I_{Na} activated at each test potential from a holding potential of −109 mV (Fig. 4*C*), by the driving force, using an extrapolated reversal potential of +71 mV for I_{Na}. A Boltzmann function fitted to the data points (Fig. 4*D*) yielded a voltage of half-maximal activation (V_{act}) of −60 mV and a slope (V_s) of 5 mV. I_{Na} inactivated fully over a 30-ms test pulse and recovery from inactivation followed an exponential time course which had a time constant of 6.9 ms at −89 mV. The voltage dependence of steady-state inactivation (or availability) of I_{Na} was determined using 30-ms conditioning pulses to potentials between −109 and +11 mV, followed by a test depolarization to −39 mV. A Boltzmann curve fitted to the mean test I_{Na} yielded a voltage of half-maximal inactivation (V_{inact}) of −94 mV and a slope factor of −10 mV (Fig. 4*E*). Superposition of the normalized activation Boltzmann curve on the inactivation curve revealed an overlap centred at −70 mV suggesting the presence of a small 'window current' (Fig. 4*E*, filled region).

Voltage-gated outward K^+ currents

The outward K^+ current recorded in SCs filled with K^+ internal solution (2.5–11 mM EGTA) activated at test potentials positive of about −40 mV and was characterized by a 'noisy' appearance at potentials positive of +10 mV (Fig. 5*A*). I_K showed little inactivation over 160 ms and was inhibited by 70% by 2 mM TEA ($n = 3$) and by 74% by 5 mM TEA ($n = 3$) (Fig. 5*A*), indicating that over 70% of I_K is generated by the opening of TEA-sensitive K^+ channels. These channels were the large-conductance Ca^{2+}-activated (BK) channels whose activity was recorded from four outside-out patches. Application of TEA (2–5 mM) to the bathing solution markedly inhibited the currents through these BK channels and in the presence of 5 mM TEA, there was evidence that SCs also express TEA-resistant K^+ channels of a smaller conductance (Fig. 5*B*i and ii). Application of charybdotoxin (CHTX; final bath concentration, 166 nM) to two excised patches also blocked

currents through the BK channels in the patch (Fig. 5*C*i and ii) and unmasked the smaller conductance channel. The latter may underlie the TEA-resistant component of I_K in whole-cell recordings (Fig. 5*A*).

BK channel openings were recorded in almost all cell-attached patches and were active at the 'resting' potential of SCs, that is, when V_p was 0 mV (Fig. 5*D*i). The frequency of openings and the amplitude of the unitary current (i) increased as V_p was made more negative (Fig. 5*D*i). The unitary conductance (γ) of these BK channels averaged 237 ± 10 pS ($n = 7$) while the V_p at which i was zero averaged -43 ± 3 mV ($n = 7$) (Fig. 5*D*ii). This indicates that the 'resting' potential of SCs (V_m) in OE slices is around -51 mV, with the LJP correction

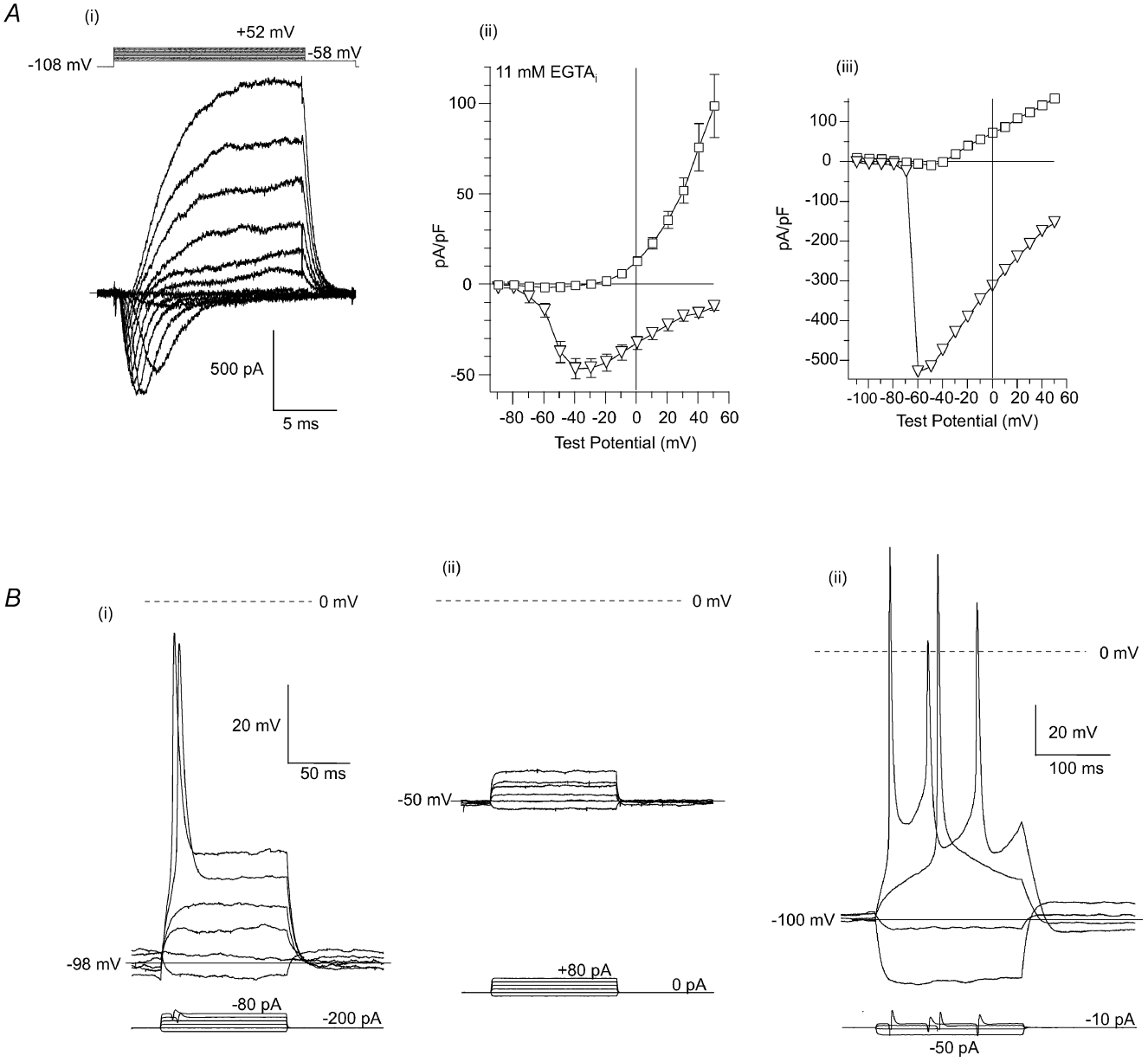

Figure 3. Density of net voltage-gated currents in SCs and an ORN and their regenerative activity
Cells were internally dialysed with KF solution (11 mM EGTA). *A*i, net inward and outward currents (lower traces) triggered by 15 ms step depolarizations to potentials indicated (upper traces). ii, current density of inward and outward currents, normalized to C_{cell}, recorded from SCs and plotted as a function of test potential. Data points represent means of 11–18 SCs. iii, current density of inward and outward currents for an ORN. *B*i, current clamp recording from a SC showing single action potential upon depolarization to −60 mV from a holding potential of about −98 mV. ii, in the absence of a holding current (lower traces), the SC depolarized to −50 mV and lacked regenerative activity. iii, current clamp recording from an ORN. Injection of hyperpolarizing current revealed the presence of a weak depolarizing sag in the electrotonic response, characteristic of ORNs (Vargas & Lucero, 1999), while depolarizing current pulses triggered bursts of action potentials.

Cell-attached recordings were also obtained from SCs that had been treated with 18β-glycyrrhetinic acid (18β-GA, 20 μM) which blocks a resting leak conductance (see below). The unitary conductance of BK channels in the 18β-GA-treated cells was unchanged (211 ± 5 pS, $n = 9$) but zero-current potential was shifted some 20 mV negative to $V_p = -64 \pm 3$ mV ($n = 9$) and V_m was hyperpolarized to -72 mV.

We noted that in cell-attached recordings, the magnitude of the unitary BK channel currents and their opening frequency increased spontaneously in the form of bursts, 5–10 s in duration (Fig. 5*E*i). In the recording depicted in Fig. 5*E*ii, the amplitude of the single-channel current increased from 4.2 to 9 pA during the burst. Using the slope conductance derived from BK channel openings between bursts, we estimated that the membrane potential of this SC was likely to have hyperpolarized by approximately 15 mV at the peak of the burst (Fig. 5*E*iii).

The resting 'leak' conductance of SCs

Compared with ORNs, SCs have a disproportionately low R_m when normalized to C_{cell}: SCs, 11 ± 1 MΩ pF^{-1} ($n = 156$); ORNs, 137 ± 22 MΩ pF^{-1} ($n = 9$). This is largely due to the influence of a resting 'leak' conductance (g_L) in SCs that gives rise to an inward leak current (I_L) at negative potentials (Fig. 6*A*i) while in ORNs no such I_L is evident (Fig. 6*B*i). ORNs on the other hand generate a much larger I_{Na} than SCs (Fig. 6*B*ii). As shown in Fig. 6*A*ii, I_L deactivated at potentials negative to -70 mV over 1–3 s resulting in about a 2-fold increase in R_m. The voltage dependence of g_L was determined by dividing the end of pulse I_L by the driving force. In the cell

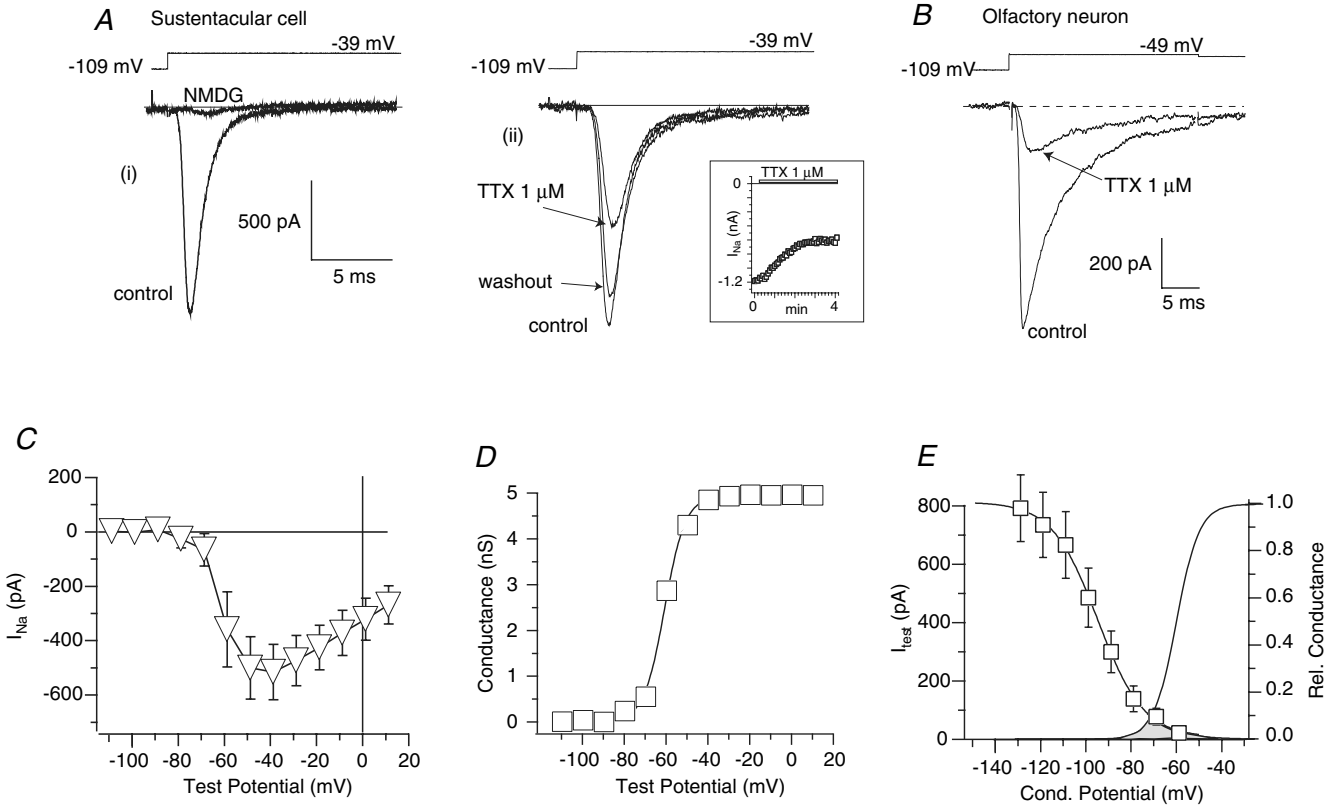

Figure 4. Properties of the voltage-gated inward Na^+ current (I_{Na}) in SCs

*A*i, substitution of Na^+ in the Ringer solution with NMDG all but abolished the I_{Na} (lower traces). ii, I_{Na} was reversibly decreased by ~50% by 1 μM tetrodotoxin (TTX). Inset shows time course of inhibition of I_{Na}. *B*, I_{Na} recorded from an olfactory neurone ($C_{cell} = 2.3$ pF), before and after treatment with TTX (1 μM) which decreased I_{Na} by 86%. *C*, current–voltage (*I–V*) relationship of the average I_{Na}. *D*, Na^+ conductance (g_{Na})–voltage curve derived from I_{Na} in panel *C*. g_{Na} was half-maximally activated at -60 mV and the fitted Boltzmann curve had a slope of 5 mV. The general form of the Boltzmann equation used was:

$$Y = Y_{max}/(1 + \exp(-(V_m - V_{0.5})/V_s) + Y_o,$$

where $V_{0.5}$ is either V_{act} or V_{inact}, V_m is the membrane potential, and Y_{max} is either the maximal conductance or maximal test current, V_s is the slope factor and Y_o is the offset. *E*, the availability of I_{Na} triggered by a test pulse to -39 mV is plotted as a function of the potential of a preceding 30 ms conditioning pulse. Mean data points are fitted with a Boltzmann curve which yielded a voltage of half-maximal availability of -94 mV and a slope factor of -10 mV. Superimposed is the normalized activation Boltzmann curve which revealed a 'window current' at -70 mV (shaded region).

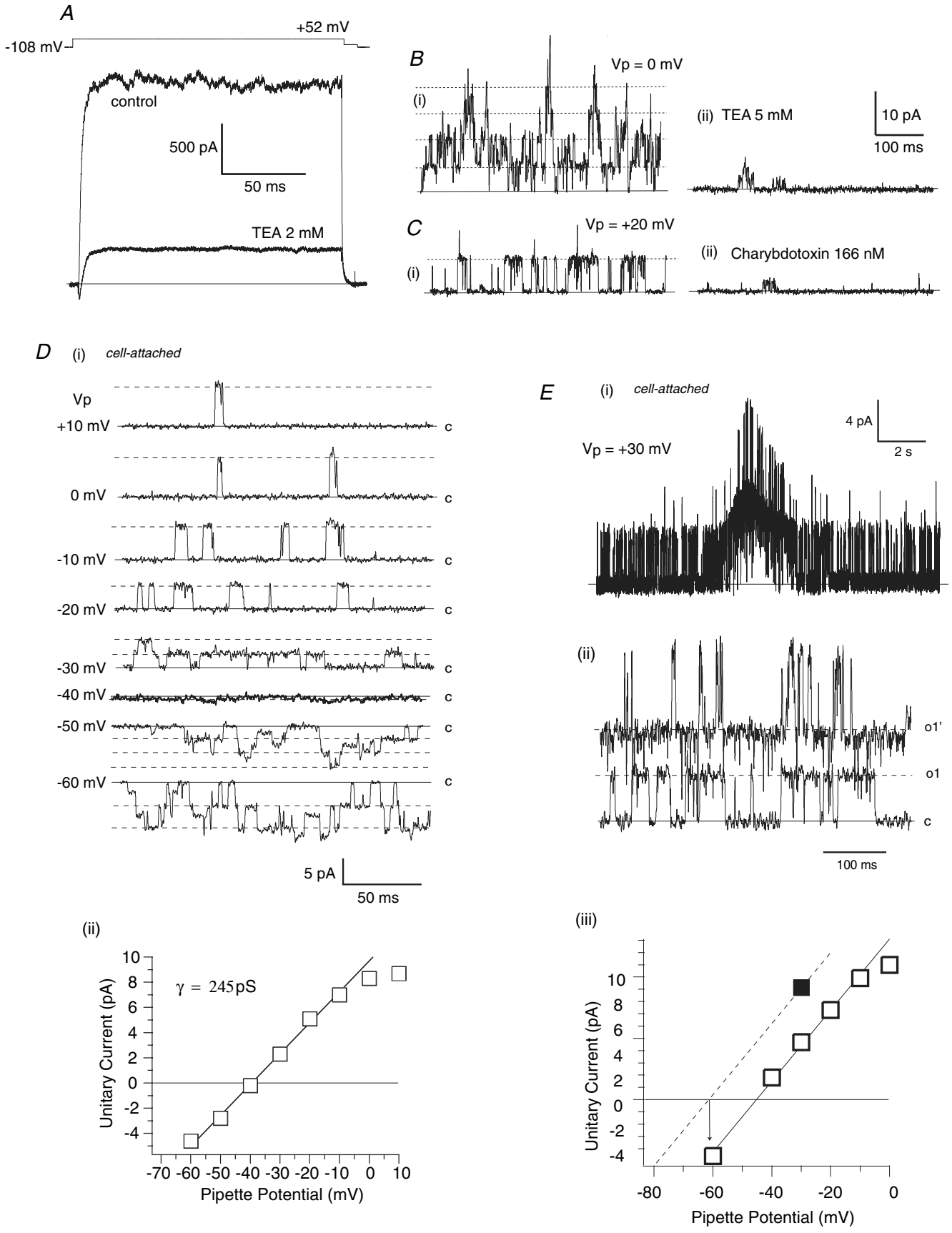

depicted in Fig. 6*A*i, E_{rev} of I_L was −14 mV (Fig. 6Aii) and a Boltzmann curve fitted to the data points yielded a voltage of half-maximal deactivation of −102 mV and a slope factor of 23 mV, while only 49% of the conductance deactivated (Fig. 6*A*iii). Overall, g_L determined from the mean values of I_L recorded in 10 Cs^+-filled cells, half maximally deactivated at −104 mV with the slope factor set to 25 mV, and 52% of g_L remained active at potentials negative of −149 mV (see Fig. 8*B*ii, □).

The pooled data from SC recordings indicated that R_m was slightly higher in Cs^+-filled cells (2.5 mM $EGTA_i$) (183 ± 25 MΩ, $n = 54$) at $V_h = -79$ mV, than in cells filled with K^+ (2.5–11 mM $EGTA_i$) (136 ± 19 MΩ, $n = 32$) ($P = 0.09$, unpaired t test) at $V_h = -78$ mV. This suggests that there may be a small resting g_K at these potentials but that g_L conducts both monovalent cations about equally. To establish that g_L is permeable to cations, Na^+ in the Ringer solution was substituted with NMDG, a larger cation that poorly permeates cation-selective channels. In four Cs^+-filled SCs, I_L recorded at −149 mV was decreased from −963 ± 314 pA in Ringer solution to −282 ± 69 pA in NMDG-Ringer solution (Fig. 7*A*i and ii) and E_{rev} was shifted from −18 to −38 mV (both values corrected for LJPs) (Fig. 7*B*i). The NMDG-sensitive component of I_L was revealed by subtracting the polynomial curve fitted to the mean data points of I_L recorded in Ringer solution, from a similar curve fitted to the mean I_L recorded in NMDG-Ringer solution (Fig. 7*B*i, continuous curve). This difference curve represents the component of I_L that was inhibited by NMDG. The NMDG-sensitive current also showed outward rectification and reversed at +2 mV. The NMDG *I–V* relationship plotted in Fig. 7*B*i is actually displaced by 2 mV relative to the *I–V* in Ringer solution along the voltage axis, to account for the change in LJP between the two solutions. A similar shift in E_{rev} was seen in six K^+-filled SCs when external Na^+ was substituted with NMDG (from −26 to −47 mV) and I_L at −148 mV was decreased from −587 ± 118 to −352 ± 75 pA. The identical shifts in E_{rev} of I_L in Cs^+- and K^+-filled cells following replacement of external Na^+ with NMDG indicates that g_L is about equally permeable to Cs^+ and K^+ but is less so to NMDG. Given a 21 mV shift in E_{rev} of I_L following substitution of Na^+ with NMDG, the relative permeability of NMDG to Na^+ (P_{NMDG}/P_{Na}) is 0.4.

It is also possible that g_L is permeable to F^- and Cl^-. If so, I_L would be diminished or blocked by substituting internal F^- and Cl^- with a larger organic anion. We therefore recorded currents from SCs filled with sodium gluconate (145 mM) in place of KF/KCl. The *I–V* relationship of I_L averaged from five SCs filled with internal gluconate indicated that E_{rev} was −52 mV when corrected for the LJP. This indicates that I_L is also dependent in part on internal F^- and Cl^-. The difference between the E_{rev} of I_L in gluconate-filled cells and the E_{rev} of I_L recorded in cells filled with CsF/CsCl (− 12 mV) indicates that the permeability of g_L to gluconate *versus* F^-/Cl^- ($P_{gluc}/P_{F/Cl}$) is 0.13. The magnitude of I_L recorded in the gluconate-filled cells (Fig. 7*B*ii, ■) was about half the magnitude of I_L recorded in cells filled with CsF/CsCl (Fig. 7*B*ii, □). The difference current, obtained by subtraction of polynomial fits to the respective data points, indicated that the gluconate-sensitive component of I_L also shows outward rectification and reverses close to +10 mV (Fig. 7*B*ii, continuous line), or +2 mV if the initial LJP is subtracted. These data suggest that g_L is permeable to both monovalent cations and anions.

Pharmacology of I_L

The voltage dependence g_L and the incomplete deactivation of I_L at negative potentials, as well as the broad ionic permeability of g_L, suggested that this current might be generated by the opening of connexon hemichannels (Ebihara *et al.* 2003). We found that I_L was substantially decreased by 18β-GA (20 μM), a specific blocker of connexons (Davidson & Baumgarten, 1988) (Fig. 8*A*i and ii, and *B*i, ■). At a test potential of −149 mV, I_L in 10 representative Cs^+-filled SCs averaged −626 ± 183 pA in control Ringer solution and −170 ± 27 pA in 22 similarly filled SCs pretreated with 18β-GA, a 76% difference in current. The decrease in current was significant ($P < 0.05$,

Figure 5. Characterization of the voltage-gated outward K^+ (I_K) current in SCs
A, whole-cell recording from a SC filled with KF showing activation of I_K upon depolarization (upper trace). External TEA (2 mM) decreased the 'noisy' I_K current by ∼80% and revealed a TEA-resistant component. *B*i, recording from an outside-out patch at V_p of 0 mV. Pipette contained KF internal solution and the bath was perfused with Ringer solution. ii, external TEA abolished the openings of the large conductance (BK) channels and revealed sparse openings of TEA-resistant channels. *C*i, recording from another outside-out patch, $V_p = +20$ mV. ii, external charybdotoxin blocked the openings of the BK channels, and unmasked a smaller conductance channel. *D*i, segments of recordings from a cell-attached patch. Dashed lines indicate open channel current, while 'c' denotes closed level. Note increase in channel openings with increasing V_p. ii, the magnitude of the unitary current (*i*) is plotted *versus* V_p. A regression line fitted to the data points (excluding those at 0 and +10 mV) yielded a unitary conductance (γ) of 245 pS while the current was zero at V_p of −41 mV. Resting potential of cell was therefore −49 mV, with LJP correction. *E*i, cell-attached patch recording from another SC, showing spontaneous increase in the activity of BK channels. ii, expanded recordings showing superimposed unitary currents taken before (o1) and during the peak of the activity burst (o1′). Closed level is denoted by 'c'. iii, *I–V* relationship of the BK channel derived from openings between bursts (□). Continuous regression line yields a conductance of 257 pS. The larger unitary current during the burst at $V_p = +30$ mV (■) indicates that the cell had hyperpolarized by 15 mV (arrow).

unpaired *t* test) at test potentials between −39 and −149 mV. The *G*–*V* relationship of the 18β-GA-sensitive I_L had a similar voltage of half-maximal activation (−106 mV) as the I_L recorded in untreated SCs (Fig. 8*B*i and ii) which indicates that 18β-GA blocks the underlying g_L or leak channels.

We also found that 9-AC (0.5 mM), a blocker of ClC-1 channels, decreased I_L in 11 K^+-filled SCs by about 40%, from −546 ± 99 pA to −330 ± 32 pA ($P < 0.05$, paired *t* test), at test potentials between −138 and −148 mV ($P < 0.05$, paired *t* test) (Fig. 8*C*) while niflumic acid (0.5 mM), another Cl^- channel blocker, also significantly decreased I_L ($P < 0.05$, paired *t* test) at test potentials between −88 and −148 mV by between 64 and 75% (Fig. 8*D*). In addition, niflumic acid increased I_K in K^+-filled SCs at potentials positive to −50 mV, as indicated by difference curve in Fig. 8*D*. Although these data suggest that a portion of I_L may be generated by a Cl^- conductance (g_{Cl}), any such conductance should be already inhibited by the internal F^- which is generally less permeant than Cl^- through Cl^--selective channels (Pusch *et al.* 1999). This suggests that 9-AC and niflumic acid may inhibit g_L.

Discussion

General properties of sustentacular cells in the olfactory epithelium of neonatal mice

We have demonstrated in the present study that sustentacular cells (SCs) can be patch-clamped *in situ*

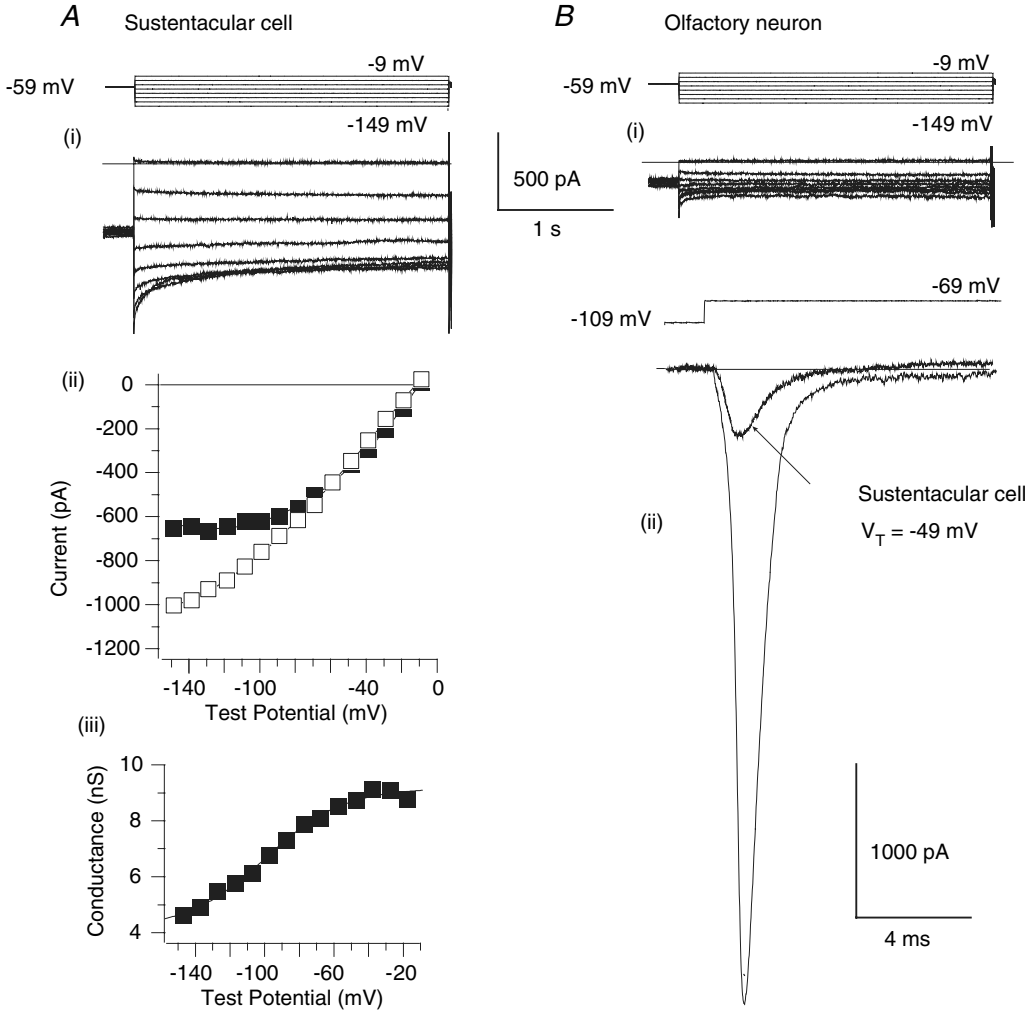

Figure 6. Voltage-dependent gating of the 'leak' current (I_L)
*A*i, typical recording of I_L in a SC showing time-dependent deactivation of the current during 2.8-s step hyperpolarizations to potentials negative of −70 mV. ii, *I*–*V* relationships of I_L recorded in the same cell, at the onset (□) and at the end of the pulse (■). iii, the I_L at each potential was converted to conductance (g_L) by dividing the current by driving force. g_L is plotted as a function of test potential (V_T). The data points are fitted with a Boltzmann curve which yielded a V_{act} of −102 mV and a slope factor of 23 mV, while 51% of the current failed to deactivate. *B*i, recording from an olfactory neurone showing little or no I_L present under similar conditions as in panel *A*, with the exception that the ORN was filled with KF and not CsF. ii, the large amplitude of the I_{Na} identified this cell as a neurone. Superimposed is the largest I_{Na} recorded from the SC depicted in panel *A*. Olfactory neurones have a much higher density of I_{Na} than SCs which have a disproportionately lower input resistance.

in tissue slices from the OE of neonatal (P0–P4) mice. When filled with fluorescent dyes, key morphological features were revealed but few if any SCs were found to be dye-coupled as both Lucifer Yellow and Alexa Fluor 488 remained confined to the patched cell. We also found that SCs generate voltage-gated Na^+ and K^+ currents that support action potential firing but the Na^+ current was largely inactivated at the resting potential of SCs in slices. This was due to the presence of an outwardly rectifying resting 'leak' conductance that drove their resting potential positive.

Voltage-gated Na^+ and K^+ currents in SCs

Sustentacular cells generated a 'noisy' outward K^+ current that activated at potentials positive of −40 mV and showed

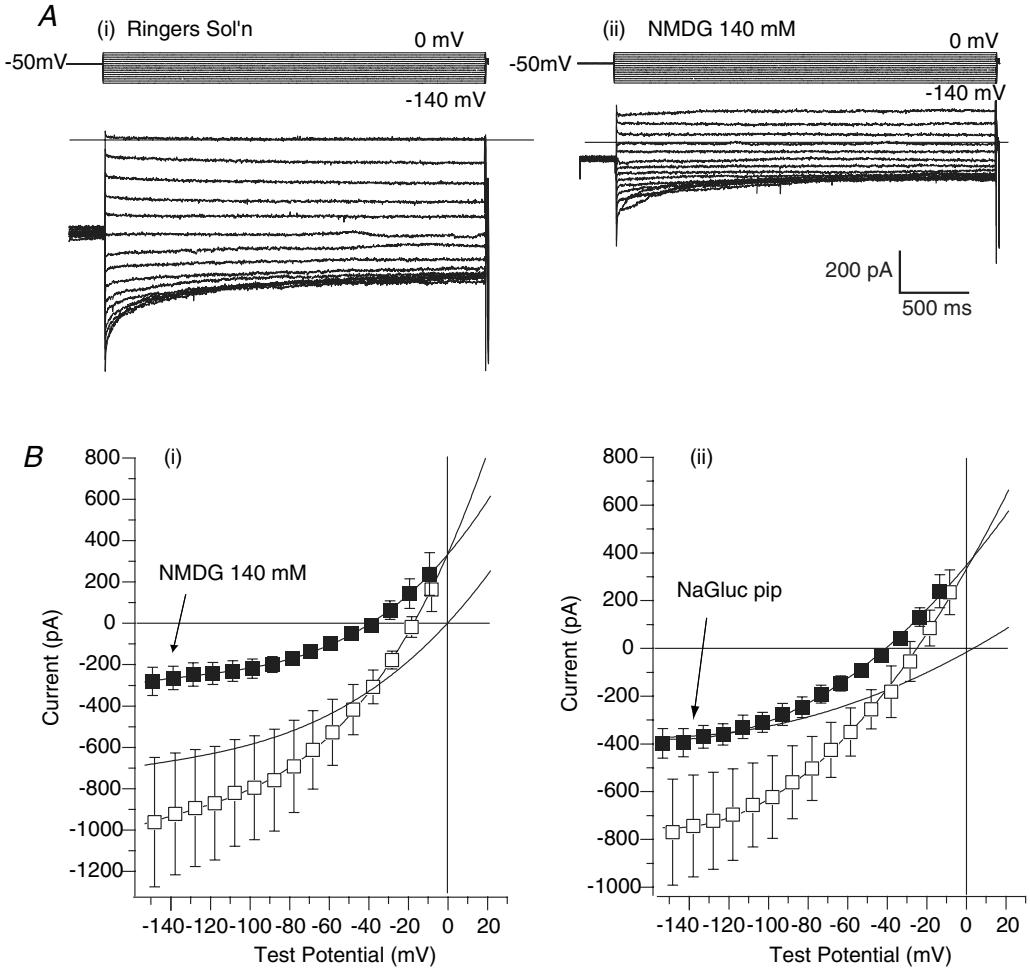

Figure 7. Ionic nature of I_L in SCs

*A*i, series of I_L (lower traces) elicited by 2.8-s test pulses to a range of potentials (upper traces), in the presence of normal Ringer solution. ii, perfusion of the cell with NMDG (140 mM)-containing Ringer solution markedly decreased I_L elicited over the same voltage range. *B*i, average *I–V* relationship of I_L in four cells filled with CsF internal solution and perfused with Ringer solution (□) and in the presence of NMDG-Ringer solution (■). The data points were fitted with polynomial functions (superimposed) which were used to generate the NMDG-sensitive current shown as a continuous curve that does not overlie the data points, which showed outward rectification. ii, average *I–V* relationship of I_L recorded in 8 cells filled with sodium gluconate internal solution and perfused with Ringer solution (■). When corrected for the LJP, E_{rev} of the I_L was −52 mV. Also plotted are the data points for I_L recorded from 10 different SCs loaded with CsF/CsCl (□) that have been similarly fitted with a polynomial. The 'gluconate-sensitive' current (continuous curve deviating from data points) was generated by subtraction of the two fitted polynomial curves, and showed outward rectification. Note that the data points for I_L recorded in gluconate-filled cells are displaced 5 mV negative to those recorded in cells filled with CsF/CsCl, to account for the difference in LJP under the two recording conditions.

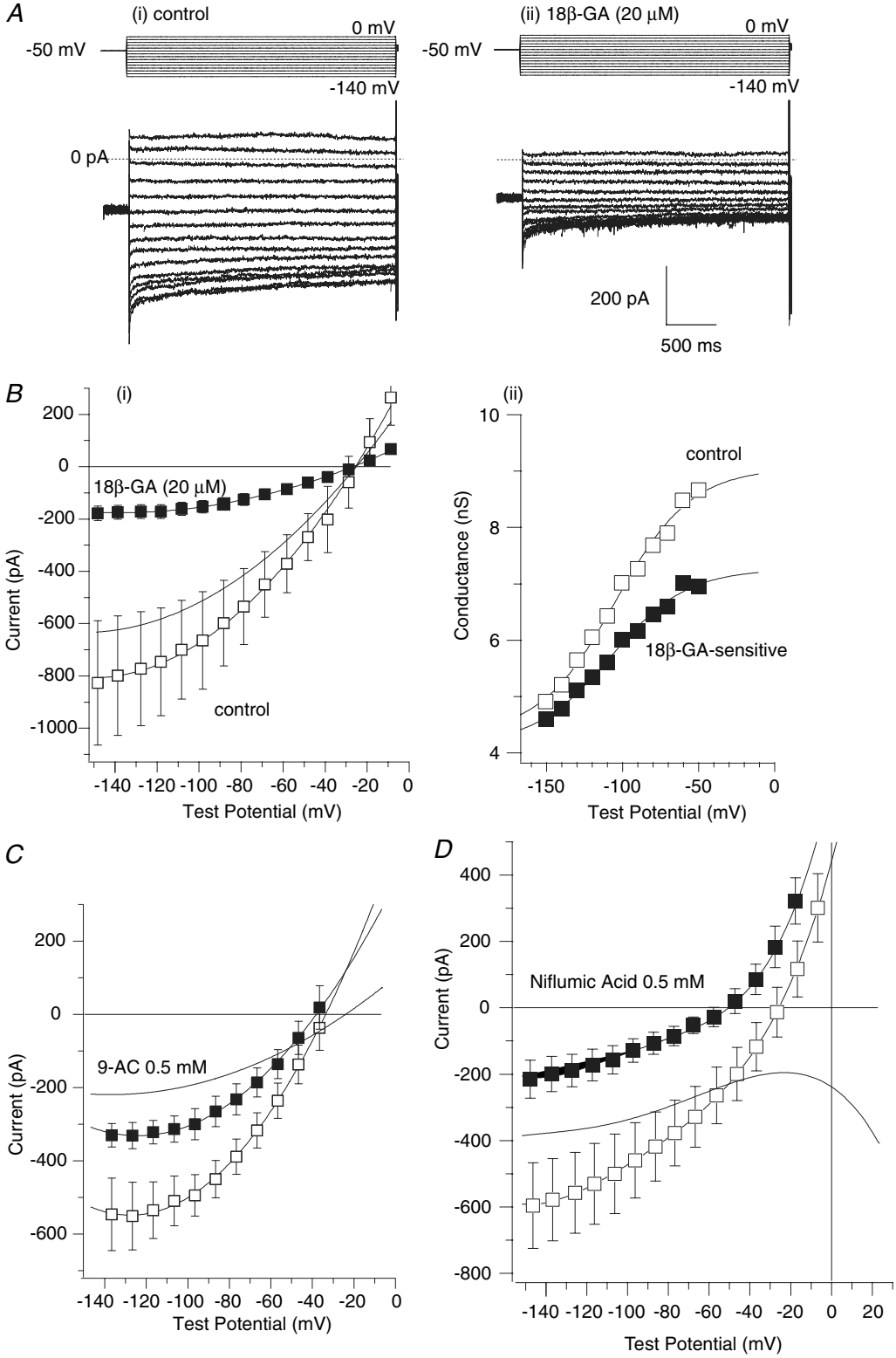

Figure 8. Pharmacology of the 'leak' current (I_L) in SCs
*A*i, the cell was filled with CsF internal solution and perfused externally with Ringer solution. From a holding potential of −50 mV, the membrane potential of the cell was stepped through a series of potentials for 2.8 ms, every 15 s and the resultant I_L was recorded (lower traces superimposed). I_L deactivated during test pulses negative of about −70 mV. ii, application of 18β-GA (20 μM) to the slice resulted in a marked reduction in I_L. *B*i, *I–V* relationships of I_L recorded in untreated SCs ($n = 10$) and in 22 SCs that had been treated with 18β-GA (20 μM; ■). The reversal potential of I_L was −12 mV. The data points have been fitted with polynomials and the difference

little inactivation over 160 ms. This current was blocked by low (2–5 mM) concentrations of TEA and recordings from membrane patches indicated that it was generated by the opening of charybdotoxin-sensitive BK channels. This result contrasts with the K^+ channels that underlie the bulk of the whole-cell K^+ current in SCs from the VNO, which were reported to be resistant to charybdotoxin (Ghiaroni *et al.* 2003). We did record openings of TEA- and charybdotoxin-resistant K^+ channels in patches, but these were relatively infrequent. Thus BK channels, under our recording conditions, are likely to generate the bulk of the K^+ current in olfactory SCs.

The density of the whole-cell BK-channel current, however, was probably underestimated in our whole-cell recordings because cells were dialysed internally with a high concentration (11 mM) of EGTA to buffer Ca^{2+}. This conclusion is supported by the fact that BK channels were invariably active at membrane potentials negative of −50 mV in cell-attached recordings while outward current was only detectable at potentials positive to −40 mV in whole-cell recordings. We attempted to use a lower concentration of EGTA (0.5 mM) to buffer $[Ca^{2+}]$ to submicromolar levels but this resulted in an irreversible increase in R_s within 1–2 min of whole-cell access, an effect that we attribute to the mobilization of vacuoles and vesicles lying adjacent to the apical surface membrane of SCs (Getchell *et al.* 1988). We noted that in cell-attached patches, BK channels often opened in bursts and this was associated with hyperpolarization of the cell, as the unitary current increased. This suggests that in non-dialysed SCs cytoplasmic or submembrane $[Ca^{2+}]$ fluctuates with time, perhaps due to the passage of Ca^{2+} waves (Hegg *et al.* 2005).

Peak current density of I_{Na} in olfactory SCs was similar to that reported in the SCs of the VNO, between 30 and 40 pA pF^{-1} (Ghiaroni *et al.* 2003). As in the VNO, I_{Na} of SCs was less sensitive to TTX than I_{Na} in ORNs which may indicate that the molecular composition of Na^+ channels in SCs differs from those expressed in neurones in both the VNO and the OE. Na^+ channels were inactivated at the resting potential of SCs, which was deduced to be about −50 mV, although we noted the possible presence of a 'window current' (5–10% of peak g_{Na}) at −70 mV. In contrast to SCs in the VNO (Ghiaroni *et al.* 2003), the density of Na^+ channels in olfactory SCs was sufficient to enable them to fire a single action potential, but this was only possible when the membrane potential was held negative to −80 mV. In cell-attached recordings, we were unable to record action currents from SCs suggesting that under resting conditions, SCs are not excitable. The probable reason for this is that Na^+ channels are inactivated at the resting potential of SCs which is maintained depolarized by an omnipresent 'leak' conductance, g_L. As for the location of Na^+ channels, since I_{Na} was adequately clamped and our recordings were obtained mainly from the cell bodies of SCs, these channels are likely to be situated on the soma, although their presence in the process cannot be ruled out.

A clear difference between SCs and ORNs in current clamp was the fact that ORNs were able to fire repetitively (up to 3–4 action potentials) when they were depolarized to suprathreshold potentials whereas SCs fired only a single action potential at the onset of depolarization. The much larger density of I_{Na} in ORNs is probably one reason for their ability to fire repetitively as it would take longer to exhaust the available Na^+ channels to the point where action potentials could not be launched. In SCs on the other hand, it is likely that the majority of the Na^+ channels inactivate during the initial action potential. Another possible explanation for the inability of SCs to fire repetitively, is the presence of g_L. This conductance which is half-deactivated at −100 mV, would switch on during the upstroke of the action potential and remain activated, thereby forcing the membrane potential positive to a level where an equal and opposite K^+ current is activated. In SCs filled with K^+, this potential is between −40 and −50 mV, at which Na^+ channels would remain inactivated.

Properties of the resting 'leak' conductance in SCs

A characteristic feature of g_L in SCs was that it deactivated (up to 50%) at potentials negative to −70 mV, such that R_m doubled when cells were held negative to −140 mV. It should be pointed out that the value of R_m that we have reported (∼160 MΩ) at the holding potential (−78 mV) is likely to underestimate the actual R_m at these potentials because of the influence of the seal resistance (R_{seal}), which was usually between 0.5 and 2 GΩ. When corrected for a typical R_{seal} value of 1 GΩ, the actual R_m for SCs is close to 190 MΩ. For the ORNs that we recorded from, their actual R_m would increase to 2 GΩ when corrected for a 1 GΩ R_{seal} and as high as 9 GΩ for a 700 MΩ R_{seal}. This latter value is close to the values reported for dissociated ORNs from rat

current generated, as in Fig. 7*B*. ii, conductance–voltage relationship derived from I_L (□). The data points are fitted with a Boltzmann curve which yielded a V_{act} of −105 mV with a slope of 25 mV. Note that 52% of the conductance (g_L) does not inactivate. ■, the portion of g_L that was blocked by 18β-GA, plotted as a function of test potential. The Boltzmann curve fitted to these data points had a V_{act} of −106 mV with the slope fixed at 25 mV. *C*, application of 9-AC (0.5 mM) to SCs filled with KF led to a decrease in I_L. *D*, under similar conditions as in panel *C* but in different cells, application of niflumic acid (0.5 mM) decreased I_L but also enhanced the outward K^+ current at potentials positive of −40 mV, as indicated by the failure of the difference current to reverse over the same voltage range.

(Lynch & Barry, 1989) and mouse OE (Maue & Dionne, 1987) and for frog ORNs (Pun & Kleene, 2004) and points out the importance of accounting for R_{seal} in cells with high R_{in} values. These corrected values further highlight the strong influence of g_L in SCs.

The slope of the *G–V* relationship of the deactivating component of g_L (~25 mV) indicated that the translocation of about one e^- was associated with deactivation of a 'leak' channel, suggesting the presence of a voltage-dependent gate. We found that g_L is about equally permeable to Cs^+, K^+ and Na^+ but that it is also likely to pass anions such as Cl^- and F^-. In isolated SCs enzymatically dissociated from the VNO, Ghiaroni *et al.* (2003) also reported that those cells possess a resting conductance that was more permeable to Cl^- than Na^+ and K^+, although the magnitude of the resting conductance of dissociated SCs of the VNO was 10-fold lower (0.6 nS) than what we report here for olfactory SCs (> 6 nS). Our data tend to support their conclusion about the ionic permeability of the resting conductance, because the E_{rev} of I_L recorded in SCs filled with gluconate was some 40 mV more negative than the E_{rev} of I_L recorded in cells filled with mainly F^-, while substitution of external Na^+ with NMDG shifted the E_{rev} of I_L by only −21 mV. However, these conclusions are only valid if one assumes that NMDG and gluconate do not permeate the leak channels.

This broad permeability of g_L and its characteristic voltage dependence suggests that I_L is generated by the opening of unopposed gap junction channels, or hemichannels. Like I_L, currents generated by hemichannels also partly deactivate to varying degrees at potentials negative to zero (Trexler *et al.* 1996; Ebihara *et al.* 2003) and their permeability to substances is based largely on molecular size. Due to this property and likely interactions between permeant ions, the GHK model of ionic selectivity cannot be readily applied (Harris, 2001). Accordingly large molecules that diffuse slowly through hemichannels may retard the passage of ions of smaller size, thus reducing the overall conductance. This may explain why in the present study, substitution of external Na^+ with NMDG or replacement of internal F^- and Cl^- with gluconate, resulted in a reduced conductance as well as in a shift in E_{rev}. The fact that the NMDG-sensitive difference current reversed at +10 mV and not at +80 mV, as would be expected if a highly Na^+-selective conductance were eliminated, suggests that NMDG may permeate the leak channels at a slower rate than Na^+ and in the process retard the passage of other ions such as F^- and Cl^-.

An important finding that strongly suggests that g_L of SCs is generated by the opening of connexon hemichannels was that application of 18β-GA, an extract from licorice that blocks connexons (Davidson & Baumgarten, 1988) caused about a 3- to 4-fold increase in R_m of SCs. This inhibition was slow to develop and required > 20 min to reach steady-state and once I_L was blocked, 18β-GA did not appear to wash out from the slice over the time course of a typical experiment (2–3 h). In addition we found that I_L was inhibited by 9-AC and niflumic acid, two compounds that are used to block Cl^- channels. Their inhibitory effects on I_L occurred at concentrations that are about 10-fold higher than the concentrations used to block Cl^- channels, although it should be noted that niflumic acid and other related fenamates have been reported to inhibit hemichannels (Harks *et al.* 2001; Eskandari *et al.* 2002).

Functional significance of voltage-gated conductances and electrical coupling in SCs

Compared with ORNs, SCs play no direct role in odour sensation. Most conspicuously, however, SCs provide structural support for ORNs and form a barrier that protects the cell bodies of ORNs from noxious agents in the nasal cavity. In light of these functions, the presence of voltage-gated ionic conductances would seem superfluous. Moreover the presence of a 'leak' conductance that clamps the membrane potential of SCs to potentials where Na^+ channels remain inactivated, would further exclude these channels from having a functional role in electrical signalling. BK channels, however, are likely to be active at rest and are probably involved in the efflux of K^+ across the apical surface of SCs. Their high density in membrane patches from the apical surfaces of SCs suggests that if BK channels are confined to this region, then it would enable SCs to establish vectorial K^+ transport. According to this scheme, K^+ in the interstitium would be actively transported into SCs at their distal processes and K^+ would then be shunted out into the nasal cavity by the Ca^{2+}-stimulated opening of BK channels on the apical surface.

At present, it is not known whether the magnitude of g_L in SCs in neonatal mouse OE slices is as large or if g_L is even present in olfactory SCs of adult mice. For technical reasons related to the preparation of slices from adult animals and likely difficulty in obtaining gigaseals, this type of study may not be possible. However, the study of Ghiaroni *et al.* (2003) in dissociated SCs from the VNO of adult mice indicates the those SCs have a much higher input resistance (1.7 GΩ) than we report here for olfactory SCs, although VNO SCs also possess a resting leak conductance of a similar ionic nature to g_L. Part of the reason that dissociated SCs from the VNO have a higher input resistance is that they have half the cell capacitance, and therefore cell surface area, of olfactory SCs *in situ*. Whether this is because the membrane processes that may contribute to a larger capacitance and lower input resistance are removed from SCs during dissociation is unclear. It is also possible that SCs from the VNO may have an intrinsically lower resting leak conductance. These possibilities need to be addressed in further studies.

Differences in input resistances between dissociated adult SCs and those *in situ* in neonatal OE may also be due to differences in the extent of electrical coupling between

SCs. The presence of electrical coupling would lower the apparent input resistance of SCs while in dissociated cells, the removal of the coupling conductance would be expected to increase their input resistance. Thus further studies are required to determine the electrical properties of isolated SCs, dissociated from the OE of neonatal mice.

An unexplored possibility in the OE is the involvement of the hemichannels that appear to underlie the resting g_L in the non-vesicular release of factors and neuromodulators. This property of hemichannels has been proposed in other systems including astrocytes in the CNS (Bennett *et al.* 2003; Saez *et al.* 2003). The openings of hemichannels themselves may also be regulated by factors intrinsic to the OE or by intracellular second messengers or metabolites (Saez *et al.* 2003). Should any of these factors reduce g_L, they may hyperpolarize SCs to a level where Na^+ channels become available to open and support action potential firing. The nature of these regulatory factors and the role of action potentials in SCs remains to be established.

References

Barry PH & Diamond JM (1970). Junction potentials, electrode standard potentials, and other problems in interpreting electrical properties of membranes. *J Membr Biol* **3**, 93–122.

Bennett MV, Contreras JE, Bukauskas FF & Saez JC (2003). New roles for astrocytes: gap junction hemichannels have something to communicate. *Trends Neurosci* **26**, 610–617.

Davidson JS & Baumgarten IM (1988). Glycyrrhetinic acid derivatives: a novel class of inhibitors of gap-junctional intercellular communication. Structure-activity relationships. *J Pharmacol Exp Ther* **246**, 1104–1107.

Ebihara L, Liu X & Pal JD (2003). Effect of external magnesium and calcium on human connexin46 hemichannels. *Biophys J* **84**, 277–286.

Eskandari S, Zampighi GA, Leung DW, Wright EM & Loo DD (2002). Inhibition of gap junction hemichannels by chloride channel blockers. *J Membr Biol* **185**, 93–102.

Getchell TV & Getchell ML (1982). Physiology of vertebrate olfactory chemoreception. In *Fragrance Chemistry*, pp. 1–25. Academic Press, Inc, New York.

Getchell ML & Mellert TK (1991). Olfactory mucus secretion. In *Smell and Taste in Health and Disease*, ed. Getchell TV, Doty R, Bartoshuk L, Snow JB, pp. 83–95. Raven Press, New York.

Getchell ML, Zielinski B & Getchell TV (1988). Odorant and autonomic regulation of secretion in the olfactory mucosa. In *Molecular Neurobiology of the Olfactory System*, ed. Margolis FL, Getchell TV, pp. 71–98. Plenum Publishing Coop, New York.

Ghiaroni V, Fieni F, Tirindelli R, Pietra P & Bigiani A (2003). Ion conductances in supporting cells isolated from the mouse vomeronasal organ. *J Neurophysiol* **89**, 118–127.

Harks EG, de Roos AD, Peters PH, de Haan LH, Brouwer A, Ypey DL, van Zoelen EJ & Theuvenet AP (2001). Fenamates: a novel class of reversible gap junction blockers. *J Pharmacol Exp Ther* **298**, 1033–1041.

Harris AL (2001). Emerging issues of connexin channels: biophysics fills the gap. *Q Rev Biophys* **34**, 325–472.

Hegg CC, Greenwood D, Huang W, Han P & Lucero MT (2003). Activation of purinergic receptor subtypes modulates odor sensitivity. *J Neurosci* **23**, 8291–8301.

Hegg CC & Lucero MT (2001). ATP evokes Ca^{2+} increases and inward currents in mouse olfactory receptor neurons. *Chem Senses* **26**, 1073.

Hegg CC, Vogalis F & Lucero MT (2005). Sustentacular cells: more active than we ever imagined. *Chem Senses* (in press).

Hille B (1992). *Ionic Channels of Excitable Membranes*, 2nd edn, pp. 341–348. Sinauer Assoc., Inc, Sunderland, MA.

Lynch JW & Barry PH (1989). Action potentials initiated by single channels opening in a small neuron (rat olfactory receptor). *Biophys J* **55**, 755–768.

Ma M, Chen WR & Shepherd GM (1999). Electrophysiological characterization of rat and mouse olfactory receptor neurons from an intact epithelial preparation. *J Neurosci Meth* **92**, 31–40.

Maue RA & Dionne VE (1987). Patch-clamp studies of isolated mouse olfactory receptor neurons. *J General Physiol* **90**, 95–125.

Pun RY & Kleene SJ (2004). An estimate of the resting membrane resistance of frog olfactory receptor neurones. *J Physiol* **559**, 535–542.

Pusch M, Jordt SE, Stein V & Jentsch TJ (1999). Chloride dependence of hyperpolarization-activated chloride channel gates. *J Physiol* **515**, 341–353.

Saez JC, Contreras JE, Bukauskas FF, Retamal MA & Bennett MV (2003). Gap junction hemichannels in astrocytes of the CNS. *Acta Physiol Scand* **179**, 9–22.

Trexler EB, Bennett MV, Bargiello TA & Verselis VK (1996). Voltage gating and permeation in a gap junction hemichannel. *Proc Natl Acad Sci U S A* **93**, 5836–5841.

Trotier D (1998). Electrophysiological properties of frog olfactory supporting cells. *Chem Senses* **23**, 363–369.

Vargas G & Lucero MT (1999). Dopamine modulates inwardly rectifying hyperpolarization-activated current (I_h) in cultured rat olfactory receptor neurons. *J Neurophysiol* **81**, 149–158.

Verkhratsky A & Steinhauser C (2000). Ion channels in glial cells. *Brain Res Brain Res Rev* **32**, 380–412.

Vogalis F, Hegg CC & Lucero MT (2005). Electrophysiology of sustentacular cells in mouse olfactory epithelium (OE). *Chem Senses* (in press).

Acknowledgements

This study was supported by the NIH NINDS (N507938); NIDCD (DC02994 to M.T.L. and DC04953 to C.C.H.).